All-printed cell counting chambers with on-chip sample preparation for point-of-care CD4 counting

Dorothee Wasserberg[a], Xichen Zhang[a], Christian Breukers[a], Bridgette J. Connell[b], Ellen Baeten[c], Dorine van den Blink[c], Èlia Solà Benet[a], Andries C. Bloem[c], Monique Nijhuis[b], Annemarie M.J. Wensing[b], Leon W.M.M. Terstappen[a], Markus Beck[a],*

[a] *Medical Cell Biophysics, MIRA Institute for Biomedical Technology and Technical Medicine, Faculty of Science and Technology, PO Box 217, 7500 AE Enschede, The Netherlands*
[b] *University Medical Center Utrecht, Department of Medical Microbiology, Virology, Heidelberglaan 100, 3584CX Utrecht, The Netherlands*
[c] *University Medical Center Utrecht, Laboratory of Translational Immunology, Section Diagnostics, Heidelberglaan 100, 3584CX Utrecht, The Netherlands*

ARTICLE INFO

ABSTRACT

We demonstrate the fabrication of fully printed microfluidic CD4 counting chips with complete on-chip sample preparation and their applicability as a CD4 counting assay using samples from healthy donors and HIV-infected patients. CD4 counting in low-income and resource-limited point-of-care settings is only practical and affordable, if disposable tests can be fabricated at very low cost and all manual sample preparation is avoided, while operation as well as quantification is fully automated and independent of the skills of the operator. Here, we show the successful use of (inkjet) printing methods both to fabricate microfluidic cell counting chambers with controlled heights, and to deposit hydrogel layers with embedded fluorophore-labeled antibodies for on-chip sample preparation and reagent storage. The maturation process of gelatin after deposition prevents antibody wash-off during blood inflow very well, while temperature-controlled dissolution of the matrix ensures complete antibody release for immunostaining after the inflow has stopped. The prevention of antibody wash-off together with the subsequent complete antibody release guarantees a homogeneous fluorescence background, making rapid and accurate CD4 counting possible.

We show the successful application of our fully printed CD4 counting chips on samples from healthy donors as well as from HIV-infected patients and find an excellent agreement between results from our method and from the gold standard, flow cytometry, in both cases.

1. Introduction

Despite the various global healthcare organizations' and many countries' concerted efforts, there are still more than 2 million new human immunodeficiency virus (HIV) infections per year, adding to the more than 36 million people currently living with HIV, many of whom are not aware of their HIV status (UNAIDS, 2017). The extent of this pandemic, especially when considering that HIV prevalence is still highest in resource-limited sub-Saharan Africa, calls for very low-cost and simple point-of-care (rapid) diagnostic tests to diagnose and stage HIV. HIV staging in point-of-care settings is done by means of CD4 counting, i.e. the enumeration of CD4 positive helper T-lymphocytes (CD4$^+$ T-cells), if viral load testing is not affordable (Ford et al., 2015). Despite the WHO recommendation to treat every HIV infected patient with antiretroviral therapy (ART)(World Health Organization, 2016),

the CD4 count is still the criterion for initiation of ART in many countries if the concentration of CD4$^+$ T-cells falls below a threshold concentration that differs between countries in the range between 200 μL^{-1} and 500 μL^{-1} (IAPAC, 2015),

The gold standard, flow cytometry is a suitable, reliable technique, when operated by experienced users, in well-controlled laboratories. However, traditional flow cytometers are bulky, fragile and expensive and can therefore not fulfill the needs of rural areas with limited access to basic infrastructure and centralized laboratories. A large number of point-of-care CD4 counting devices and techniques have been reported and reviewed recently (Damhorst et al., 2013; Glynn et al., 2013). Reported examples, besides miniaturized, dedicated flow cytometers (Manasa et al., 2007; Mossoro-Kpinde et al., 2016; Pattanapanyasat et al., 2008), are based on a wide variety of principles, including cell counting assays based on optical detection (Aitchison et al., 2012;

Alere, 2010; BDBiosciences, 2017; Cheng et al., 2007a; Daneau et al., 2017; Gao et al., 2010; Gebremicael et al., 2017; Gurkan et al., 2011; Hosokawa et al., 2012; Rodriguez et al., 2005; Sysmex Partec, 2011; Zhu et al., 2008), label-free impedance measurements of cell lysates (Cheng et al., 2007b; UNITAID - World Health Organization, 2012), or even simpler methods, like volumetric estimation of cell counts (Boyle et al., 2012) or lateral flow type assays (UNITAID - World Health Organization, 2015). Most devices fulfill many, but never all, of the World Health Organization (WHO)'s ASSURED (Affordable, Sensitive, Specific, User-friendly, Rapid and robust, Equipment-free, Delivered) criteria (UNITAID - World Health Organization, 2015) for point-of-care CD4 counting technology and to date, none of these commercially available point-of-care assays has proven simple, cheap and reliable enough to have become widely established (Pham et al., 2016; Wade et al., 2014).

We, therefore, see the greatest opportunity for improvement in simplifying sample preparation as well as reducing price per test (i.e. cost of disposables/reagents). In our opinion, a successful point-of-care CD4 counting assay for resource-limited settings should fully integrate all sample preparation (including reagents) on a disposable testing chip without the need for manual or automated external intervention. Sample handling should be restricted to the loading of the chips and not require any precision pipetting or specific skill sets, while at the same time minimizing the risks of excessive/extended handling of patient material. The fabrication of the disposable (counting chambers and materials) should be done using a low-cost method, which is also capable of high volume production.

On-chip sample preparation with integrated (dry) reagent storage on chip using diverse methods, has been reported on in the literature (Fu et al., 2010; Gervais and Delamarche, 2009; Hitzbleck et al., 2011; Stevens et al., 2008). A large variety of concepts are based on preserving (dried) reagents by embedding them in so-called matrix materials. Such matrix materials have the additional function of controlling reagent release. Many studies have been published on the successful storage and release of viable biomolecules from both, naturally and synthetically derived hydrogels off-chip (Brandl et al., 2010; Ganta et al., 2008), while the preservation of viable biomolecules on-chip has been abundantly proven, either via encapsulation/embedding (Puchberger-Enengl et al., 2014; Tijero et al., 2015; Zhu, 2008) or covalent immobilization(Gurkan, 2011; Jang et al., 2012; Luk et al., 2012; Zhao et al., 2015). Clearly, hydrogels are well-suited to act as matrix materials to preserve biological reagents and control their release in microfluidic devices (Beck et al., 2012; Cosson and Lutolf, 2014; Mortato et al., 2012).

Based on this concept, we previously reported on a very simple CD4 counting method with complete on-chip sample preparation (Beck, 2012). In short, microfluidic cell counting chambers with defined chamber height are filled with finger prick blood samples making use of capillary forces without external flow control. All reagents (fluorophore-labeled antibodies for staining) necessary for sample preparation are already embedded in a dry hydrogel matrix (gelatin) stored in the counting chambers. The hydrogel matrix delays the release of staining agent until sample inflow is complete, thereby ensuring homogeneous reagent distribution throughout the entire chamber during incubation. The homogeneous distribution of staining agent on the mm-length scale in x- and y-direction of the chamber makes it possible for the release to solely rely on diffusion across the z-direction, i.e. the chamber height (tens of μm), to mix sample and staining agent very quickly. After incubation, the chambers are imaged in a custom-built, wide field-of-view fluorescence imager, which also performs the automated image analysis, resulting in a CD4 count (number of CD4$^+$ T-cells per μL blood). Quantification is done volumetrically exploiting the fact that the imaged volume (chamber height × image area) is known. However, this proof-of-principle still relied on labor-intensive manual chip manufacturing, making low-cost high volume production impossible.

In this work, we report on the development of low-cost fabrication

methods, with high-throughput capability to produce such low-cost and easy-to-use point-of-care CD4 counting chips, as described above. As outlined in the SI, a final price per test of €2–3 appears realistic for volume production, which is considerably below the prices of existing solutions not depending on manual sample preparation (about €5–10), and also below the price of flow-cytometry-based POC CD4 counts that do require manual sample preparation (about €3–5). Also, the estimated instrument cost (see SI for details; Fig. S9) of €3000 would be very competitive (MSF Access Campaign, 2017).

For the construction of the microfluidic counting chambers, we use two substrates with the dimensions of standard microscope glass slides as the top and bottom, as the format is readily available at low cost. To attach these two slides to each other with a well-controlled separation to form a sample chamber, we chose drop-on-demand printing of glue/spacer mixtures, because it fulfills our requirements for the fabrication well: a simple and low-cost technique, capable of both, rapid prototyping and large volume production. Printing the outline of the compartments using glue/spacer mixtures defines the geometry of the counting chambers. The glue acts as the seal for these compartments, while the spacer material determines the height of the counting chambers. We chose microbeads as spacer material, which have been used in a wide range of fields for many different types of application (Hitzbleck and Delamarche, 2013).

Another crucial component of the chip is the hydrogel matrix with embedded antibodies. Numerous methods for the automated deposition of biomolecules and commercially available systems for spray coating, inkjet printing and contact printing have been comprehensively reviewed by Hitzbleck and Delamarche, (2013) For our application, we chose inkjet printing, because it is inherently suitable for rapid prototyping and fast up-scaling, as well as patterning for future parallelization, e.g. in an array format. In addition, inkjet printing has been shown to be suitable for the deposition of macromolecules (de Gans et al., 2004; Singh et al., 2010; Tekin et al., 2008) and to be biocompatible (Tijero, 2015; Zhu, 2008).

In the following, we will discuss the (inkjet) printing methods we developed for the fabrication of fully printed CD4 counting chips and will demonstrate their successful application with samples from healthy donors as well as HIV-infected patients.

2. Materials and methods

2.1. Materials

All water samples used were of milliQ quality. All materials were used as received, unless stated otherwise. 20 μm diameter, mono-disperse non-crosslinked poly(styrene) (PS) beads (TS 20) as well as 20 μm and 30 μm diameter, monodisperse crosslinked PS beads (Calibre™, CS 20 and CS 30) from Microbeads AS (Skedsmokorset, Norway) were used suspended in UV-curable glue (Byllux 6308, viscosity: 40 mPa·s), purchased from Byla GmbH (Runkel, Germany). Gelatin (type A, 295 g Bloom) and thrombin (bovine) were purchased from Sigma-Aldrich (St. Louis, MO USA). Fluorophore-labeled antibodies, allophycocyanin-labeled antiCD3 IgG (APC-αCD3, clone SK7, 260 kDa) and peridinin-chlorophyll-labeled antiCD4 IgG (PerCP-αCD4, clone MEM241, 308 kDa), were purchased from Becton Dickinson (BD, Erembodegem, Belgium) and Exbio Praha (Exbio, Vestec, Czech Republic), respectively.

Gelatin and gelatin/antibody mixtures used as inks for printing were all filtered gravitationally prior to use, with a membrane filter (CellTrics®, mesh 20 μm, Partec, Münster, Germany). An antibody cocktail for flow cytometry (CD3/CD4/CD8/CD45 Multitest™, BD), fluorescence counting beads (Trucount™ absolute counting tubes, BD) and FACS™ Lysing Solution from BD were used according to the manufacturer's specifications. Standard microscope glass slides (76 mm × 26 mm × 1 mm, Menzel Gläser, Thermo Fisher, Waltham, MA USA) and injection molded slides made from TOPAS cyclic olefin

copolymer, ZEONEX cyclic olefin polymer, poly(styrene) and poly(methyl methacrylate) (COC, COP, PS, and PMMA respectively, 70 mm × 26 mm × 1 mm, Microfluidic Chipshop, Jena, Germany) were used. Laser-cut PMMA slides (Solaris Clear S000, PSC A/S, Brønderslev, Denmark) with holes were used for the fabrication of chambers. Prior to use, glass slides were rinsed with copious amounts of water, ethanol and acetone, and then dried under a stream of N_2, while polymer slides were rinsed with copious amounts of isopropanol and dried under a stream of N_2.

2.2. Equipment

A custom-built interferometer was used to determine chamber heights. Briefly, the light from a laser diode (λ = 405 nm) is collimated and focused at a single point of a counting chamber with two high numerical aperture lenses (diameter = focal length = 25.4 mm). The transmitted light is collimated by another lens of the same type, filtered by neutral density filters and falls onto the CCD chip of a camera. Part of the light is reflected on the inner surfaces of the chamber resulting in rings of constructive and destructive interference on the camera chip, depending on the transmission angle of the light through the chamber. Automated analysis of the resulting interferogram yields the chamber height.

The topography of gelatin/antibody layers was determined using a white light interferometer (smartWLI-microscope, GBS, height resolution ~10 nm).

Fluorescence images for image cytometry and layer characterization were recorded using a custom-built fluorescence imaging system (Beck, 2012) with wide field of view (7.8 mm × 5.2 mm) and moderate optical resolution of about 10 μm. A portable version of the above fluorescence imager (field of view: 8.9 mm × 6.7 mm, details, together with a cost estimate can be found in the SI, Fig. S9), based on the same principles with built-in, automated image analysis, was used during the analysis of patient samples.

2.3. Reagent deposition by inkjet printing

Ink preparation: To prepare solutions for inkjet printing, gelatin powder was dissolved in water at 40 °C for 1 h while stirring vigorously. To the resulting solution, 0.6 μg mL^{-1} APC-αCD3, 0.2 μg mL^{-1} PerCP-αCD4, and 100 U mL^{-1} thrombin stock solutions and water were added to yield final concentrations of 0.3%w/v of gelatin, 10 ng mL^{-1} APC-αCD3, 3 ng mL^{-1} PerCP-αCD4, and 0.6 U mL^{-1} thrombin. The solutions were left to cool to room temperature (RT), and filtered before use.

Inkjet printing: Inkjet printing was performed using an industrial inkjet printer (LP50, PixDro, Meyer Burger B.V., Eindhoven, The Netherlands) equipped with a Konica Minolta, 512MHX printhead with 512 nozzles in 2 staggered rows. Droplets of ~20 pL were dispensed onto laser cut PMMA slides with filling holes and venting slits in multiple passes (swaths) at (360 dpi)^2 resolution ("native resolution"), resulting in final resolutions between (360 dpi)^2 and (1880 dpi)^2. Unless stated otherwise, printed reagent layers were stored at 4 °C and ~10% relative humidity (RH). For further discussions of the fabrication of reagent layers, see below.

2.4. Chamber fabrication by piezo-actuated deposition

Ink preparation: 1%w/v suspensions of microbeads in UV-curable glue were prepared freshly, each day, by re-suspending aliquots of previously washed and dried microbeads.

Dispensing: For the deposition of chamber walls, a Pipejet P9 nanodispenser (Biofluidix GmbH, Freiburg, Germany) with a 200 μm orifice was used with optimized settings (Fig. S1).

Assembly: A custom-built setup was used to automatically dispense the glue/bead suspension as well as assemble and cure counting chambers on microfluidic chips. The nanodispenser was mounted on a xyz gantry (Movtec L-60) to dispense the glue/bead suspension to form the outlines of the later chamber walls. Immediately after dispensing the curable glue/bead suspension on a plastic slide (with deposited reagent layer) the grabber unit of the setup was used to automatically retrieve a glass cover slide with glass weight (65 g), place it on the freshly printed slide, leave it to settle for 5 s and cure the glue using a 405 nm Luminus CBT-90UV LED at 5 A for 1 s. For further discussions of the chamber fabrication process and parameters see below.

2.5. Evaluation of the performance of fully printed CD4 counting chambers

For an initial evaluation of our technique, we used blood from healthy donors, processed to cover the clinically relevant range of CD4 counts, while leftover patient blood was used for testing under more realistic conditions. All blood samples contained EDTA as anticoagulant. To counteract the anticoagulant and thereby reduce the effect of cell movement during imaging (discussed in detail in the SI, Fig. S11), calcium chloride (10 mM final concentration) was added to the samples immediately before use, while thrombin was already contained in the reagent release layer on the chip. This step would not be required for finger prick samples. The combined results of the two chambers per slide were compared with the reference counts from flow cytometry.

Blood samples for the first evaluation were obtained anonymously from healthy individuals at the University of Twente, all of whom had provided written informed consent in advance. Reference values for CD4 counts from healthy donors were determined using BD Multitest™ on a BD FACS ARIA II flow cytometer, according to the manufacturer's specifications. Samples with a large range of CD4 counts were prepared to determine the correlation between CD4 counts obtained using our image cytometry method with those obtained using the reference method, flow cytometry. Whole blood was first centrifuged at 1000 ×g for 15 min to separate blood plasma, leukocytes (buffy coat) and erythrocytes. After removing most of the plasma, the buffy coat was carefully aspirated and then, a pure erythrocyte fraction was collected. Subsequently, plasma and erythrocyte fractions were recombined, at a ratio of 1:1, to mimic the natural hematocrit, yielding a leukocyte depleted sample. The CD4 counts of leukocyte depleted and buffy coat samples were determined using flow cytometry (n = 3). The resulting CD4$^+$ T-cell concentrations of the leukocyte depleted and the buffy coat samples, were used to calculate mixing ratios for the two fractions resulting in a number of samples with calculated CD4 counts in the range of 5 μL^{-1} to 1400 μL^{-1}.

Left-over blood samples from HIV-infected patients, who had given written informed consent for the use of their samples for anonymous research purposes at the University Medical Center Utrecht (UMC Utrecht), were used anonymously to study the performance of our image cytometry method vs. the standard flow cytometry. Image cytometry was used to determine the CD4 counts of patient samples, for which reference CD4 counts had already been routinely determined using MultiTest™ reagents and MultiSet™ four color automated immunophenotyping software (Becton Dickinson, Erembodegem, Belgium) on a FACS Canto II v3.0 (Becton Dickinson) flow cytometer at the UMC Utrecht. Per patient sample, two slides, each with two counting chambers, were used to perform the assay either on the day the blood sample was drawn or on the following day.

3. Results and discussion

3.1. Fabrication of counting chambers by printing

As discussed in the Introduction, we chose drop-on-demand printing of UV-curable glue containing microbeads to fabricate our counting chambers. Glue/bead mixture was dispensed onto a substrate along the outline of the intended chamber walls and then a glass slide was added as cover (Fig. 1 and Fig. 2), resulting in a sealed chamber. The diameter of the suspended monodisperse microbeads determines the chamber height (~30 μm).
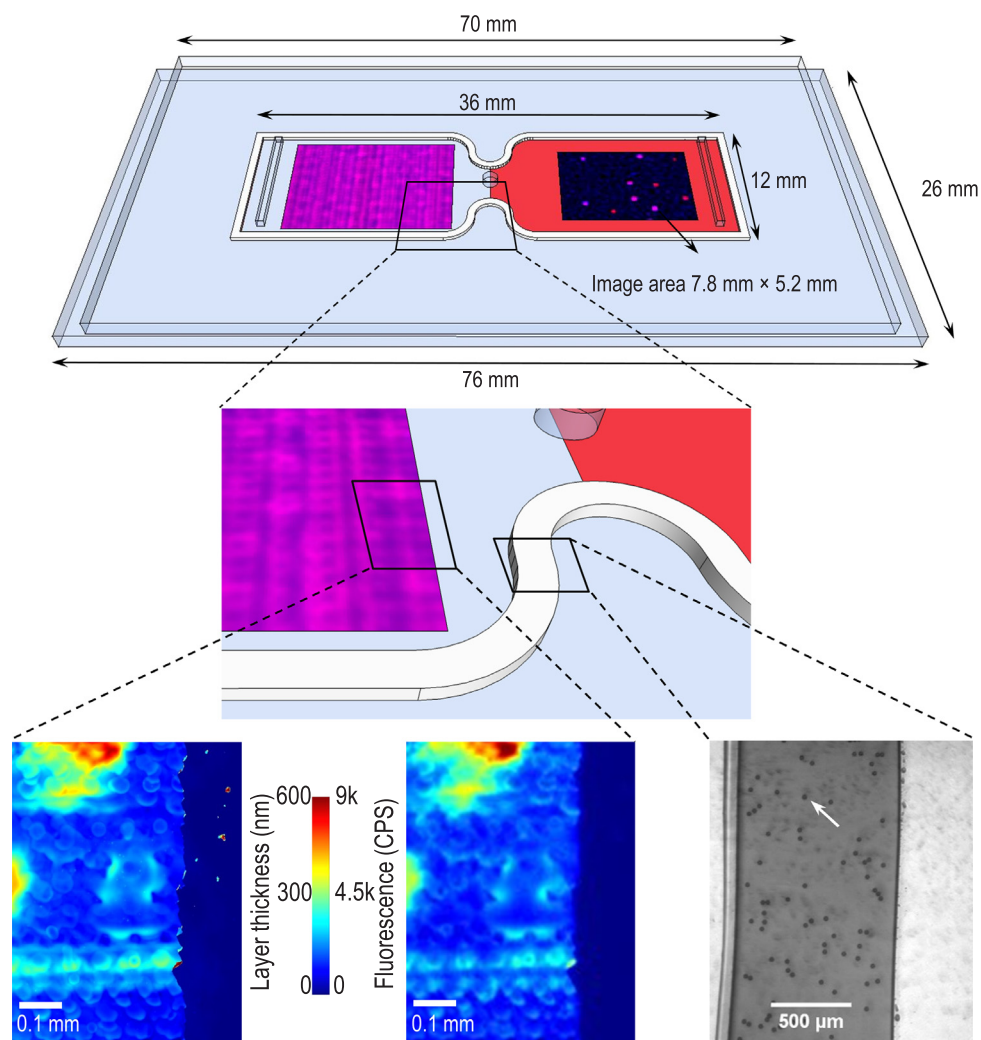
Fig. 1. Schematic representation of the chip design (top) and zoom-in (middle). In the left chamber the fluorescence image of a dry layer, and in the right chamber fluorophore-stained cells are shown as overlays of the fluorescence images of both fluorophores (APC and PerCP). Topography (bottom, left) and fluorescence image (bottom, middle, APC) of the same part of an inkjet-printed reagent layer. Bright field image (bottom, right) of a segment of a printed chamber wall. The white arrow indicates an individual microbead.

Materials for the fabrication of chambers were selected based on the following criteria: reproducibility of dispensing ink, compatibility of microbeads and glue, compatibility of glue and substrate, and control over chamber heights.

We achieved reliable drop dispensing of Byllux 6308 UV-curable glue, resulting in drop volumes of ~8 nL. Suspensions of crosslinked PS microbeads in Byllux 6308 UV-curable glue were found to be stable overnight (Fig. S2). The sedimentation of the beads in the glue was avoided by matching the densities of the two materials (1.05 g cm^{-3}).

PMMA was chosen as a substrate material to ensure that printed features would remain stable on the substrate (Furdui and Harrison, 2004; Gascoyne and Vykoukal, 2004; Stringer and Derby, 2010) (i.e. no de-wetting, Fig. S3). The print pattern was optimized to ensure the coalescing of the dispensed drops into stable printed features, i.e. uninterrupted lines (Fig. S4). The optimized parameters, 45° zig-zag print pattern, with a 0.5 mm center-to-center distance of drops, were employed for all further chamber fabrication.

The heights of the printed counting chambers produced for the use with patient samples (see Section 3.3) were determined interferometrically to be 30.5 ± 1.5 μm (n = 418). Despite the small variation in height, each chamber was labeled with a barcode encoding the actual chamber height, which was used in the image analysis to determine the exact imaged sample volume. Besides the chamber height,

the barcode also contains information about the type of the assay (APC-αCD3/PerCP-αCD4), production day and a unique identifier.

3.2. Inkjet printing of reagent storage and release layers

We employed inkjet printing for the fabrication of a thin layer of gelatin as matrix, in which the staining agents were embedded. The gelatin matrix has two functions: First, to minimize the degration of the fluorophore-labeled antibodies during storage in the dried layers. Second, to ensure homogeneous cell staining throughout the chamber by delaying the antibody release during blood inflow.

First, the feasibility of storing fluorophore-labeled antibodies in a gelatin matrix will be addressed. As can clearly be seen in Fig. S5, the intensity of fluorophores in the printed dry gelatin layers slowly decreases with storage time. Additionally, humid conditions lead to a larger intensity drop, confirming our previous findings (Zhang et al., 2016a). Therefore, for the evaluation of our on-chip CD4 counting method, all slides were used within 8 weeks after their fabrication.

The second function of the gelatin matrix is to control the timing of the release of staining agents into the cell counting chamber. On the one hand, the release of staining agents must be delayed until sample inflow has completed (stopped-flow configuration), which takes on the order of ~10 s. If the delay is too short, a significant fraction of antibody will
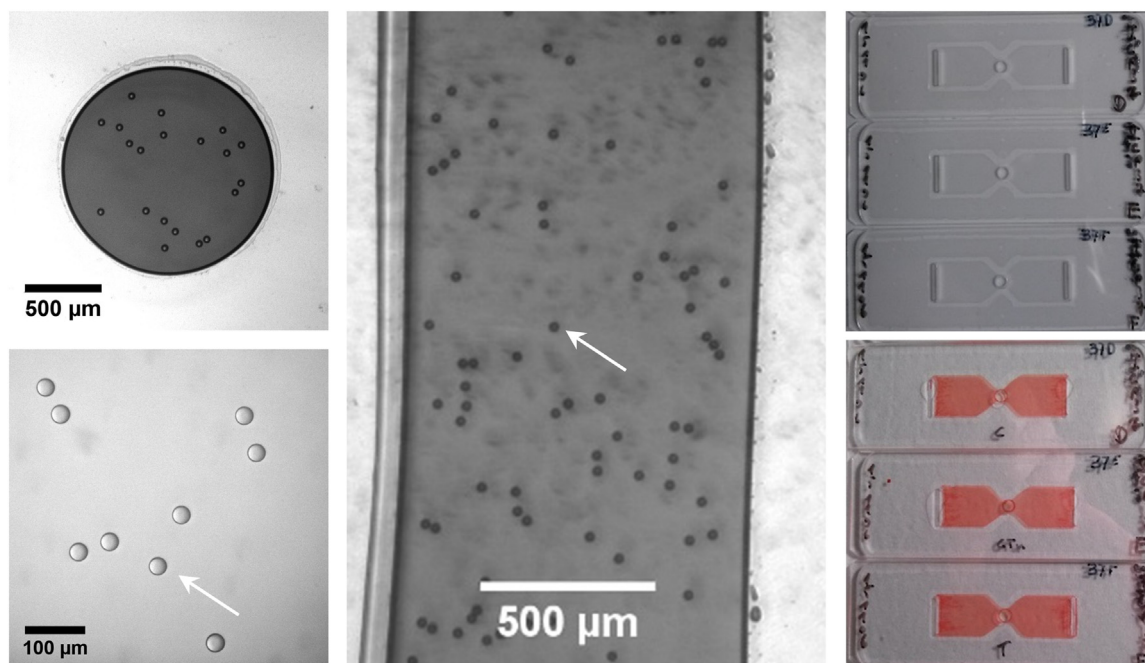
Fig. 2. Bright field images of a single drop of cured Byllux 6308 glue containing CS 30 microbeads (30 μm diameter) on a PMMA substrate covered by a glass slide (top, left); of CS 30 microbeads in cured glue (bottom, left); of a printed and cured line of glue/bead suspension being part of an assembled chamber (middle). White arrows indicate individual microbeads. A photograph of 3 consecutively fabricated chips before (top, right) and after (bottom, right) filling.

be released during sample inflow and, subsequently, be washed toward the chamber exit, causing substantial inhomogeneity in cell staining. On the other hand, the entirety of the embedded antibody must be released fast enough (< 10 min) to make rapid staining and testing within 30 min feasible, while background inhomogeneity, due to trapped antibody, is kept as low as possible.

Gelatin is well suited as a release matrix to fulfill these two conditions: First, dry gelatin/antibody layers take up water from the in-flowing sample, causing a swelling of matrix and with it a gradual increase of antibody release. This characteristic of the matrix effectively slows down initial release, causing the necessary delay of antibody release during blood inflow. Second, in its fully swollen state (equilibrium swelling ratio ~14 ×), gelatin layers are capable of rapid release of the majority of embedded antibody, well within the first 10 min after sample inflow. Antibody release from gelatin layers has previously been determined to take place on the order of tens to hundreds of seconds for a few hundred nm thick layers (Zhang et al., 2016b).

In order to translate our earlier results, gathered on cast layers (Zhang, 2016b), to printed gelatin/antibody layers, the first step was the development of a method to print gelatin/antibody layers that are as homogeneous as possible, with regard to both topography as well as fluorescence intensity. Obviously, homogeneous staining can best be achieved above a topographically homogeneous release layer, especially in a stopped-flow configuration. Additionally, the more homogeneous the distribution of antibody in the layer, the higher the signal to noise ratio, improving sensitivity.

As a first step, the topographical homogeneity of printed pure gelatin layers was optimized. The following conditions were found to be essential to ensure reproducible and stable jetting of aqueous gelatin solutions, using a Pixdro LP50 printer equipped with a Konica Minolta KM512 printhead: A KM512MHX printhead with intermediate nozzle diameter (~27 μm) was selected as a compromise between maximized resolution and minimized shear forces, see below. The concentration of gelatin was kept constant at 0.3%w/v. Furthermore, the clogging of nozzles due to drying had to be prevented by, first, always using all 512 nozzles; second, keeping the print speed ≥ 5 mm s^{-1} and third, avoiding active heating of substrate and printhead. Complying with the

aforementioned prerequisite settings, we developed an inkjet printing procedure for the fabrication of (pure) gelatin layers with optimized topographical homogeneity.

In previous work, we analyzed kinetic release data and found that the results fit well with a diffusion-controlled release model (Zhang, 2016b). This means that antibody release from gelatin layers is strongly dependent on the thickness of the gelatin matrix. Based on our earlier results, we used thicknesses of gelatin/antibody layers in the range of few hundred nm as a starting point for optimization. Layers of such thicknesses had proven to represent a compromise between sufficient initial delay of release and close-to-complete release as early as possible within the incubation time of 30 min. It should be mentioned here that the released fraction of antibody on both time scales (10 s and 10 min) also depends strongly on the conditions under which the layers are formed and left to mature(Zhang, 2016a), which will be discussed in greater detail below.

We have found that, in order to fabricate topographically homogeneous, i.e. smooth, gelatin layers, the key parameter that needs to be optimized is the amount of dispensed gelatin solution per unit time, i.e. the dispensing rate. If too much solution is dispensed per unit time, there will not be sufficient time for water to evaporate, before the addition of more liquid during the next swath of the printhead. Eventually, the accumulation of solution will reach a point when it will cause a coalescing ("puddle formation") of material and, thus, topographical inhomogeneity on large (mm to cm) length scales.

To optimize the dispensing rate, we varied print speed (Fig. S6) and final resolution of the layer (Fig. 3), while keeping all other parameters influencing the amount of liquid dispensed per unit time as predetermined by the need to ensure stable jetting as mentioned above, like the resolution per swath and the concentration of gelatin. We found that a print speed of 5 mm s^{-1} (87 s per swath) was optimal (Fig. S6, left) and adopted this speed for all further printing of gelatin/antibody layers. Furthermore, layers were fabricated with final resolutions of $(360 \text{ dpi})^2$, $(1080 \text{ dpi})^2$, $(1440 \text{ dpi})^2$ and $(1800 \text{ dpi})^2$ in a single print job. The final resolution of the printed layer essentially changes the amount of dispensed material and is therefore directly correlated to the layer thickness, as shown in Fig. 3. As discussed before, an increased
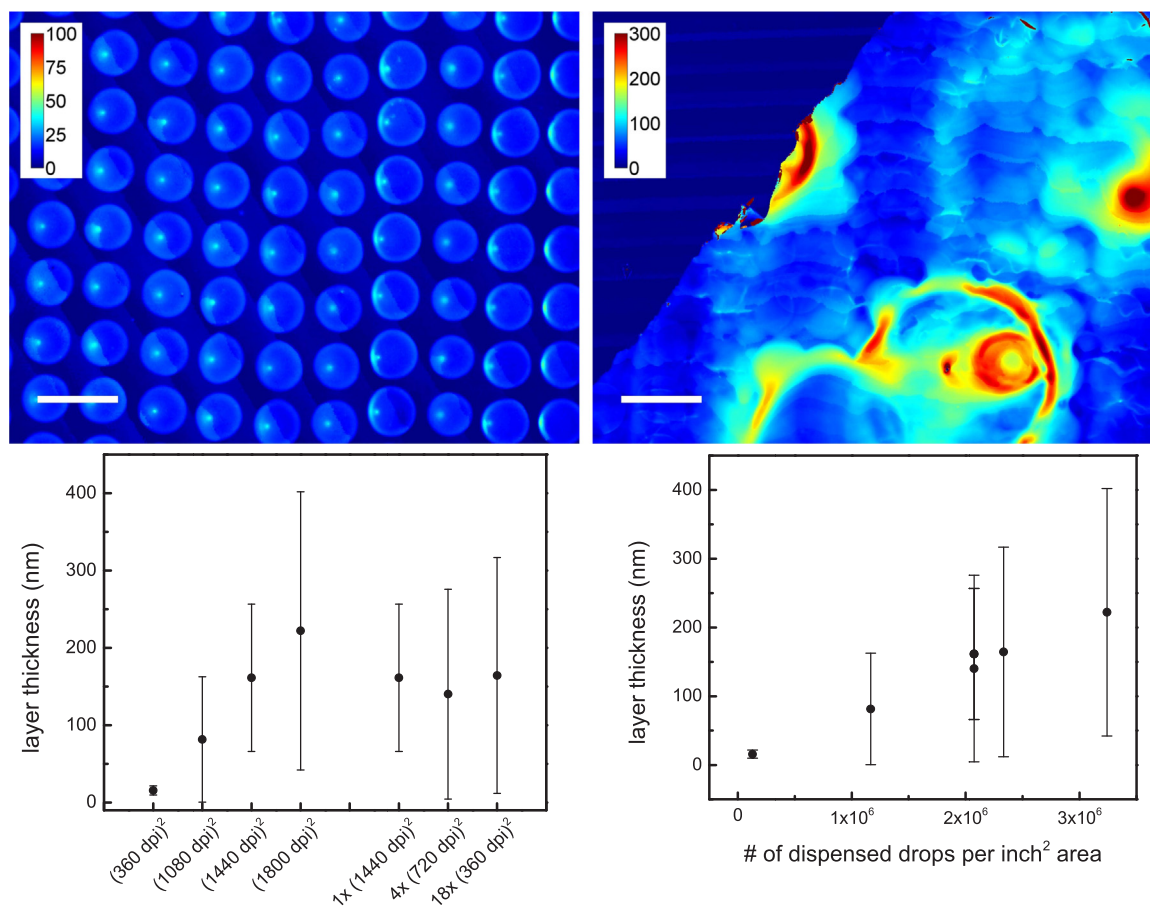
Fig. 3. Representative white light interferometry images of (single print job) gelatin layers printed at final resolutions of $(360\ dpi)^2$ (top, left) and $(1080\ dpi)^2$ (top, right). Calibration bars indicate layer thicknesses (nm), scale bars: 0.1 mm. Plot with the averaged thicknesses of the gelatin-covered areas determined from white light interferometry images (bottom, left) and the same data plotted against the number of dispensed drops per $inch^2$ (bottom, right). Data points with error bars represent averages of n ≥ 6 images (each image from a different substrate) and their respective averaged standard deviations.

substrate temperature to speed up drying, thus allowing for larger dispensing rates, was not compatible with the requirement of achieving stable jetting.

In an attempt to improve topographical homogeneity, printing gelatin layers in multiple print jobs was tested. The reasoning being that a break (≥ 1 min) between print jobs would allow for additional drying time, which was expected to improve smoothness. A layer with a final resolution of $(1440\ dpi)^2$ was selected to test this hypothesis: As the further increase of drying times between the 16 consecutive swaths of a print job did not result in further improvement (Fig. 3, bottom, left), a single print job (dispensing at 5 mm s^{-1}) was adopted as a standard printing strategy to maximize throughput and ensure stable jetting without loss of layer quality.

Having arrived at an optimized method to produce pure gelatin layers of the highest attainable topographical homogeneity, we used it to fabricated gelatin/antibody layers to optimize antibody release and, thus, cell staining.

To identify CD4$^+$ T-cells, the following fluorophore-labeled antibodies were selected as staining agents: APC-αCD3 (stains all T-lymphocytes) and PerCP-αCD4 (stains the CD4$^+$ subpopulation, i.e. helper T-lymphocytes and, weakly, monocytes), which yields the required CD4$^+$ T-cells as the double positive subpopulation after staining. The number of double positive cells, detected via image cytometry (divided by imaged volume), yields the absolute CD4 count in cells per unit volume.

Previously, we determined an optimal concentration to approach saturation of cell staining intensity (within 30 min in 30 μm high chambers) in the range of 10^8 antibody molecules per mm^2 for both

APC-αCD3 and PerCP-αCD4, corresponding to antibody concentrations in the counting chamber in the 10 nM range, consistent with equilibrium dissociation constants in the range of 1 nM (Beck, 2012; Zhang, 2016b). Therefore, all gelatin/antibody layers were fabricated, aiming at roughly 10^8 antibody molecules per mm^2 of surface area in the counting chamber for each antibody.

As mentioned above, the second function of the gelatin matrix is to ensure homogeneous cell staining. The following section will address the strategy we devised to achieve said homogeneous cell staining in detail. As discussed before, achieving homogeneous antibody release requires optimizations on two time scales: the delay of initial release during inflow as well as the complete release well within the incubation time. For our previously cast layers, a simple optimization of layer thickness provided a solution to both problems, i.e. an optimal layer thickness (~ 500 nm) could be found for which the release on both time scales (10 s and 10 min) could satisfy the criteria for homogeneous, saturated cell staining. However, analysis of the kinetics of antibody release from printed gelatin layers, revealed drastic changes, when compared with release from cast layers. In Fig. 4, left column, kinetic release data is plotted against the square root of time. Samples of gelatin/antibody solution that had been passed through the printhead under different conditions (different power settings used for piezo actuation and/or different pressures) were all cast and their antibody release was recorded in time. As reference, the same solution was cast without having been passed through the printhead. When examining the release kinetics more closely, it becomes clear that the initial phase of the release follows the square root dependence, which is expected for Fickian diffusion from a thin slab (Higuchi, 1961; Siepmann et al., 1999):
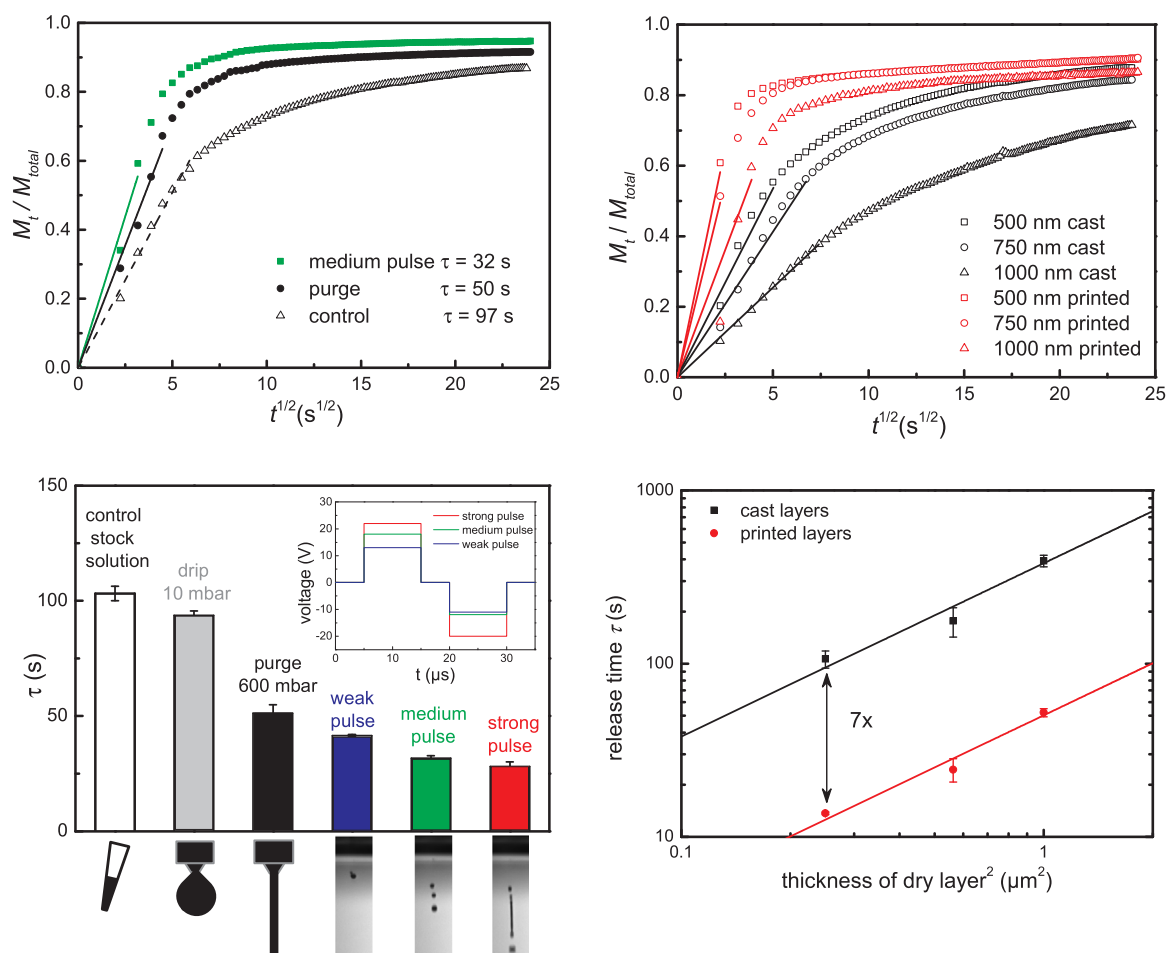
Fig. 4. Top left: kinetics of APC-αCD3 release from 500 nm thick cast layers with fits to their initial release in order to determine release times, τ. Bottom left: the resulting release times, τ, determined by measuring the release of APC-αCD3 in time, from layers cast using solutions passed through inkjet printing nozzles under the influence of shear forces of varying magnitudes (inset). As control, a solution was cast from ink from the reservoir, without having been passed through the printhead. Top right: kinetics of APC-αCD3 release from cast gelatin layers of different thicknesses with fits to their initial release in order to determine release times, τ. Bottom right: dependence of release times, τ, of APC-αCD3 from gelatin layers on dry layer thickness. Black and red lines are fits of the data according to Eq. (2). Data points represent mean ± standard deviation (n = 3).

$$\frac{M_t}{M_{\text{total}}} = \left(\frac{t}{\tau}\right)^{1/2} \tag{1}$$

where M_t is the mass released at time t, M_{total} is the total mass of antibody embedded in the layer. The process can be characterized by the release time τ, given by (Siepmann et al., 2012)

$$\tau = \frac{\pi L^2}{4D} \tag{2}$$

where L is the thickness of the layer and D is the diffusion constant. It seems that increased shear exerted on the gelatin/antibody solution, while passing through the nozzle, results in faster antibody release from the resulting layer (up to 3 times as fast).

This effect can be rationalized when considering that gelatin can undergo two types of physical crosslinking. Apart from the general physical crosslinks, which any sufficiently long macromolecule can form at sufficiently high concentrations, gelatin can form an additional type of supramolecular linkage: the partial re-forming of collagen-like triple helices (Badii et al., 2006; Djabourov and Papon, 1983; Kozlov and Burdygina, 1983). It is well established that the process of cross-linking via the formation of helical structures is slow (time scales in the range of days) and that the process depends very much on ambient conditions, like relative humidity (RH) and temperature (Badii et al., 2005; Godard et al., 1978; Yakimets et al., 2005). With this in mind, one can interpret the effect of shear forces on gelatin solutions, as

rupturing existing helical crosslinks, stretching polymer chains from coils to fully extended states and even breaking the polymer chains (Hoath et al., 2012; McIlroy et al., 2013; Wheeler et al., 2016). The resulting layers would then contain mostly incomplete coils of (partially ruptured) polymer chains with a greatly reduced number of crosslinks, effectively increasing the mesh size of the resulting layers, which in turn would result in faster antibody diffusion and, thus, faster release (Zhang, 2016a; Zhang, 2016b).

The changes of release times, τ, are even more pronounced, when directly comparing release from cast layers with release from printed layers (Fig. 4, right column). The release time, τ, of antibody released from printed layers is 7 times smaller than that of cast layers of comparable thicknesses. This additional effect may be due to the shorter drying times, when comparing printed (< 90 s per swath) and cast samples (~20 min),(Zhang, 2016b) preventing the slow formation of helical crosslinks even more effectively. Clearly, printed gelatin layers would have to be much thicker, than their cast counterparts, to achieve similar delays of initial antibody release. As has been previously determined, for a sufficient delay of initial release, a minimum release time of 100 s is required (Zhang, 2016b). However, dry printed layers would have to be more than 1.5 μm thick on average to achieve τ ≥ 100 s, which would partially block the cell counting chamber upon swelling of the layer due to layer inhomogeneity. It was therefore not possible to use diffusive release from inkjet-printed layers to achieve
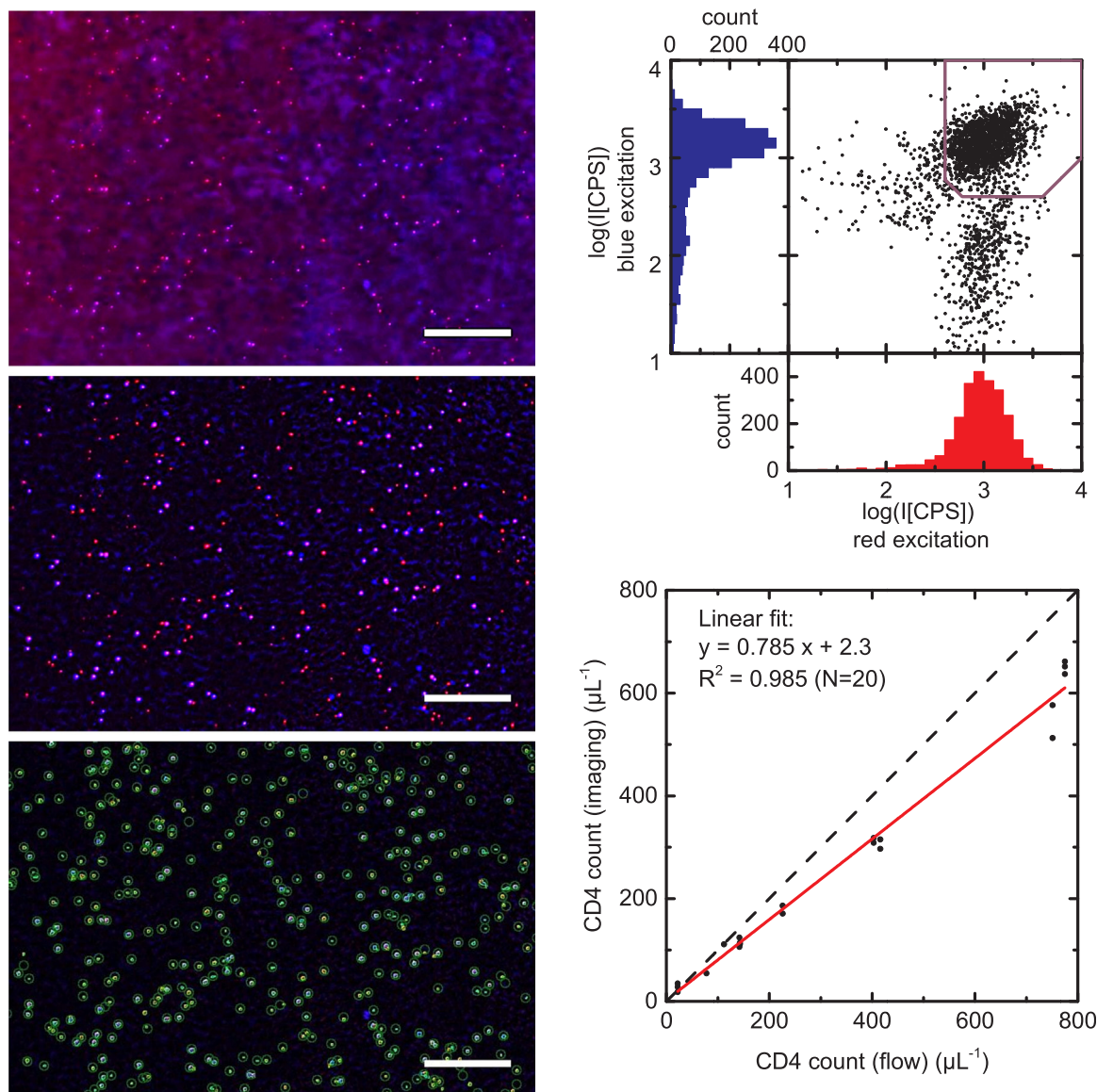
Fig. 5. Processing of overlays of fluorescence images (a chamber subject to initial and 6-week follow-up maturation with *T*-switch) recorded under blue and red excitation (Left: top, raw overlay image; middle, overlay image after background correction; bottom, overlay image with identified objects (i.e. ROIs) marked by green circles. Scale bars: 0.5 mm. In addition, image areas in which the sample moved between the two exposures (due to thermal expansion) were excluded from the analysis based as described in the SI. Right: top, scatter plot and histograms of the fluorescence intensities under blue vs. red excitation of all identified objects; bottom, comparison of average absolute, uncalibrated CD4 counts obtained from two (partially leukocyte depleted) samples from healthy donors (whole blood containing EDTA and CaCl$_2$), using image and flow cytometry. (For interpretation of the references to color in this figure legend, the reader is referred to the web version of this article.)

sufficient delay of the release and at the same time reliable sample inflow. We, then, chose to use a final resolution of (1080 dpi)^2 (average thickness ~80–100 nm) in combination with a method we devised earlier(Zhang, 2016a), to treat the printed layers such that they effectively prevent antibody wash-off during blood inflow and allow for a complete release during incubation: First, layers were exposed to increased RH (85%) in the cold (4 °C) for two days, then left to mature further, under dry, cold conditions (Fig. S7). This treatment has been shown(Zhang, 2016a) to induce efficient formation of helical crosslinks in gelatin layers. Indeed, printed, then actively crosslinked gelatin/antibody layers, turned out to be good candidates to realize initial delay of antibody release in our CD4 counting chips (Fig. S7, open symbols). Second, complete release during incubation was also actively controlled, by "switching" the state of the swollen gelatin layers from gel to solution (*T*-switch, i.e. increasing the temperature of the chip to 40 °C for 2 min). This *T*-switch allowed for the rapid and complete release of

all remaining antibody in a layer, controlled by an external stimulus (Fig. S7, solid symbols).

These measures for controlling antibody release proved to be beneficial in our cell staining application. Fig. S8 demonstrates the effect of layer maturation and *T*-switch on homogenizing the fluorescence background in the cell counting chambers.

3.3. Performance of fully printed CD4 counting chambers

The performance of our CD4 counting chambers was assessed in two steps by the level of correlation of absolute CD4 counts obtained using our image cytometry technique, with CD4 counts obtained using flow cytometry. In the first step, blood from healthy donors, processed to cover a wide range of CD4 counts, was used, while for the second step leftover patient blood was used.

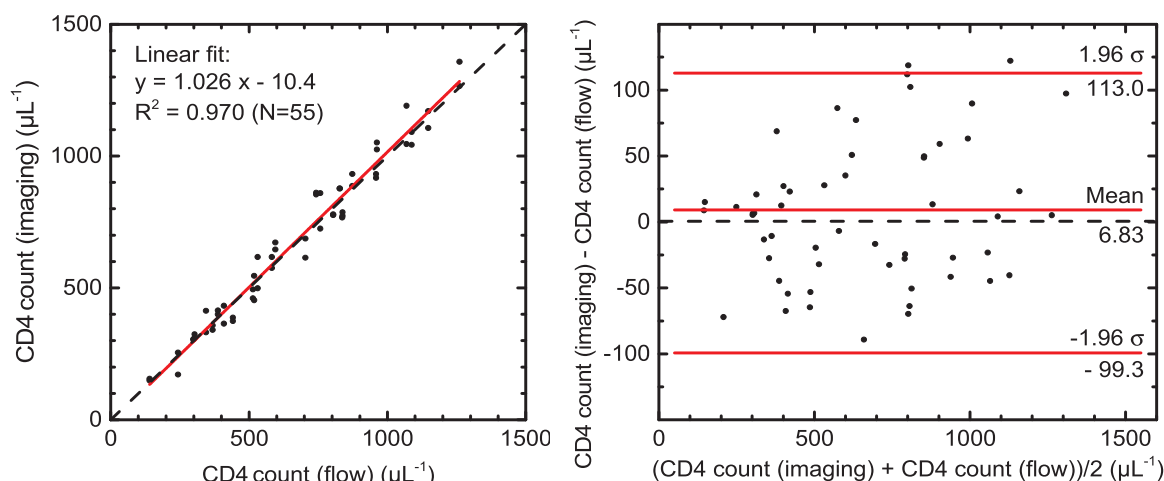First, leukocyte depleted blood samples from two healthy donors

Fig. 6. Evaluation of our CD4 counting assay using patient samples (whole blood containing EDTA and CaCl$_2$): Top: Comparison between absolute CD4 counts obtained by image cytometry using printed CD4 counting chips compared with reference counts from flow cytometry. Bottom: Bland-Altman plot of the data.

were spiked with varying amounts of their previously removed leukocytes to obtain samples with a large range of different CD4 counts. Fig. 5, left, briefly illustrates the image processing workflow, background subtraction, identification of cells, being small (3–15 pixels) round objects, and the determination of fluorescence intensities of the identified cells.

Further details of the image processing are discussed in the SI. The scatter plot (Fig. 5, top, right) resulting from image analysis yields the number of CD4$^+$ T-lymphocytes as the double positive subpopulation (CD4$^+$ and CD3$^+$, i.e. within the polygon gate displayed in the scatter plot). This number, divided by the known chamber height and image area yields the absolute CD4 count per µL. CD4 counts are plotted against the results obtained by flow cytometry and an excellent correlation was found across a wide range of CD4$^+$ T-cell concentrations (Fig. 5, bottom, right).

It should be noted that the data shown in Fig. 5, bottom right, are not calibrated. Discrepancies between the two methods originate from the choice of parameters in the image analysis with the goal to maximize the correlation between the two methods by minimizing false positives and false negatives (a more detailed discussion can be found in the SI).

Second, to substantiate this first validation, we proceeded to analyze a set of patient samples and compared our results with reference data obtained using flow cytometry.

After suitable threshold intensities were determined from a first teaching set, samples from 52 HIV-infected patients were tested, using 2 slides with 2 chambers each per patient sample. Results were obtained per slide. As a quality control, we used the average fluorescence intensities of the cells within the gate of the double positive subpopulation. Chambers were excluded if these intensities did not exceed the thresholds intensities determined before (14 of 188 chambers, resulting also in the exclusion of 2 out of 94 slides) as it indicated insufficient staining.

The first 5 samples were used to calibrate the test (Fig. S12, left) and excluded from further evaluation. Results from the samples analyzed on the day of blood draw (55 results from 28 patients) are shown in Fig. 6. Regression analysis yields a coefficient of determination of $R^2 = 0.97$ (Lin's concordance correlation coefficient (Lin, 1989) (ρ_c) = 0.984), which demonstrates an excellent agreement, which can also be seen in the Bland-Altman (Altman and Bland, 1983; Bland and Altman, 1986; Giavarina, 2015) plot (Fig. 6, bottom).

The performance on samples analyzed the day after drawing was still acceptable, but not as accurate as the samples analyzed on the same day (Fig. S12, right). As the reference counts were only obtained on the day of sampling, we cannot determine whether this is a consequence of

changing concentrations of double positive cells or whether the cell counting is less reliable with aged samples. We therefore excluded these samples from further analysis.

4. Conclusion

In summary, we have demonstrated the fabrication of fully printed microfluidic CD4 counting chips with complete on-chip sample preparation and successfully demonstrated their applicability as a CD4 counting assay for monitoring the treatment of HIV-infected patients.

We believe that CD4 counting in low-income and resource-limited point-of-care settings is only practical and affordable, if tests can be fabricated at very low cost and if all manual sample preparation is avoided, while operation as well as quantification is fully automated and independent of the skills of the operator. Such a CD4 counting method eliminates the need for expensive external equipment (disposables, pipettes, pumps etc.) and materials (reagent/lysing solutions and buffers) for sample preparation, while also precluding the reliance on trained personnel (fully automated analysis and quantification).

Our automated CD4 counting assay includes the entire sample preparation on-chip, and minimizes the required equipment to a portable image cytometer for fluorescence readout and automated analysis. Here, we have demonstrated low-cost fabrication of our CD4 counting chips via (inkjet) printing techniques, which makes upscaling to mass production straightforward.

We have developed a printing method to fabricate chamber compartments, with controlled heights, by dispensing monodisperse microbeads suspended in UV-curable glue, using a piezo-actuated nanodispenser. Furthermore, we devised an inkjet printing method to deposit hydrogel layers with embedded fluorophore-labeled antibodies, onto our microfluidic chips, for on-chip sample preparation and reagent storage.

By employing optimized printing parameters, we achieved the deposition of homogeneous gelatin/antibody layers on PMMA slides, as well as the fabrication of counting chambers with well-defined heights (30.5 µm ± 1.5 µm) containing these reagent layers.

In addition to printing, we adopted extra measures (layer maturation and *T*-switch) to precisely control antibody release (initially delayed release + temperature-triggered rapid dissolution) from printed layers for intense and homogeneous on-chip cell staining.

We successfully tested our CD4 counting chips on different healthy donors and found an excellent agreement between CD4 counts determined using our image cytometry method and using the gold standard, flow cytometry. We then proceeded to test the assay using leftover blood from HIV-infected patients and, again, found an excellent

agreement between results from our method and the reference.

We believe that our CD4 counting assay has great potential for use in low-income and resource-limited point-of-care settings, due to its extremely simple concept and low-cost production method. It allows for a short turnaround time and easy handling with a low risk of contamination. We are presently investigating, how to translate the methods described here to other essential point-of-care cell counting applications. The concept gains great flexibility and speed via the use of printing techniques for fabrication and can, therefore, be rapidly adapted to test new cell counting assays, indicating the great potential of this method for the development of future point-of-care applications.

Competing interests statement

There are no competing interests to declare.

Acknowledgements

Appendix A. Supporting information

Supplementary data associated with this article can be found in the online version at doi:10.1016/j.bios.2018.07.002.

References

Aitchison, J.S., Chen, L., Dou, J.J., Nayyar, R.K., Method and system for portable cell detection and analysis using microfluidic technology, CA2828487A1, 2012.
Alere, 2010. Pima™ Analyser User Guide. Alere, Jena.
Altman, D.G., Bland, J.M., 1983. Statistician 32 (3), 307–317.
Badii, F., MacNaughtan, W., Farhat, I.A., 2005. Int. J. Biol. Macromol. 36, 263–269.
Badii, F., Martinet, C., Mitchell, J.R., Farhat, I.A., 2006. Food Hydrocolloid. 20, 879–884.
BDBiosciences, 2017. ⟨https://www.bdbiosciences.com/documents/FACSPresto-BR.pdf⟩, (Accessed June 2018).
Beck, M., Brockhuis, S., van der Velde, N., Breukers, C., Greve, J., Terstappen, L.W.M.M., 2012. Lab Chip 12 (1), 167–173.
Bland, J.M., Altman, D.G., 1986. Lancet 1 (8476), 307–310.
Boyle, D.S., Hawkins, K.R., Steele, M.S., Singhal, M., Cheng, X., 2012. Trends Biotechnol. 30 (1), 45–54.
Brandl, F., Kastner, F., Gschwind, R.M., Blunk, T., Tessmar, J., Gopferich, A., 2010. J. Control. Release 142, 221–228.
Cheng, X., Irimia, D., Dixon, M., Sekine, K., Demirci, U., Zamir, L., Tompkins, R.G., Rodriguez, W., Toner, M., 2007a. Lab Chip 7 (2), 170–178.
Cheng, X., Irimia, D., Dixon, M., Ziperstein, J.C., Demirci, U., Zamir, L., Tompkins, R.G., Toner, M., Rodriguez, W.R., 2007b. J. Acquir. Immune Defic. Syndr. 45 (3), 257–261.
Cosson, S., Lutolf, M.P., 2014. Sci. Rep. 4, 4462.
Damhorst, G.L., Watkins, N.N., Bashir, R., 2013. IEEE Trans. Biomed. Eng. 60 (3), 715–726.
Daneau, G., Aboud, S., Prat, I., Urassa, W., Kestens, L., 2017. PLoS One 12 (1), e0170248.
de Gans, B.J., Duineveld, P.C., Schubert, U.S., 2004. Adv. Mater. 16, 203–213.
Djabourov, M., Papon, P., 1983. Polymer 24 (5), 537–542.
Ford, N., Meintjes, G., Pozniak, A., Bygrave, H., Hill, A., Peter, T., Davies, M.-A., Grinsztejn, B., Calmy, A., Kumarasamy, N., Phanuphak, P., deBeaudrap, P., Vitoria, M., Doherty, M., Stevens, W., Siberry, G.K., 2015. Lancet Infect. Dis. 15 (2), 241–247.
Fu, E., Lutz, B., Kauffman, P., Yager, P., 2010. Lab Chip 10, 918–920.
Furdui, V.I., Harrison, D.J., 2004. Lab Chip 4 (6), 614–618.
Ganta, S., Devalapally, H., Shahiwala, A., Amiji, M., 2008. J. Control. Release 126, 187–204.
Gao, D., Li, H.F., Guo, G.S., Lin, J.M., 2010. Talanta 82 (2), 528–533.
Gascoyne, P.R., Vykoukal, J.V., 2004. Proc. IEEE 92 (1), 22–42.
Gebremicael, G., Belay, Y., Girma, F., Abreha, Y., Gebreegziabxier, A., Tesfaye, S., Messele, Z., Assefa, Y., Bellete, B., Kassa, D., Vojnov, L., 2017. PLoS One 12 (4), e0176323.
Gervais, L., Delamarche, E., 2009. Lab Chip 9 (23), 3330–3337.
Giavarina, D., 2015. Biochem. Med. 25 (2), 141–151.

Glynn, M.T., Kinahan, D.J., Ducree, J., 2013. Lab Chip 13 (14), 2731–2748.
Godard, P., Biebuyck, J.J., Daumerie, M., Naveau, H., Mercier, J.P., 1978. J. Polym. Sci., Part B: Polym. Phys. 16, 1817–1828.
Gurkan, U.A., Anand, T., Tas, H., Elkan, D., Akay, A., Keles, H.O., Demirci, U., 2011. Lab Chip 11 (23), 3979–3989.
Higuchi, T., 1961. J. Pharm. Sci. 50, 874–875.
Hitzbleck, M., Delamarche, E., 2013. Chem. Soc. Rev. 42, 8494–8516.
Hitzbleck, M., Gervais, L., Delamarche, E., 2011. Lab Chip 11, 2680–2685.
Hoath, S.D., Harlen, O.G., Hutchings, I.M., 2012. J. Rheol. 56 (5), 1109–1127.
Hosokawa, M., Asami, M., Nakamura, S., Yoshino, T., Tsujimura, N., Takahashi, M., Nakasono, S., Tanaka, T., Matsunaga, T., 2012. Biotechnol. Bioeng. 109 (8), 2017–2024.
IAPAC, 2015, Global HIV Policy Watch. ⟨https://hivpolicywatch.org/⟩ (Accessed June 2018).
Jang, E., Kim, S., Koh, W.G., 2012. Biosens. Bioelectron. 31, 529–536.
Kozlov, P.V., Burdygina, G.I., 1983. Polymer 24 (6), 651–666.
Lin, L.I.-K., 1989. Biometrics 45 (1), 255–268.
Luk, V.N., Fiddes, L.K., Luk, V.M., Kumacheva, E., Wheeler, A.R., 2012. Proteomics 12, 1310–1318.
Manasa, J., Musabaike, H., Masimirembwa, C., Burke, E., Luthy, R., Mudzori, J., 2007. Clin. Vaccin. Immunol. 14 (3), 293–298.
McIlroy, C., Harlen, O.G., Morrison, N.F., 2013. J. Non-Newton. Fluid Mech. 201 (Supplement C), 17–28.
Mortato, M., Blasi, L., Barbarella, G., Argentiere, S., Gigli, G., 2012. Biomicrofluidics 6, 044107.
Mossoro-Kpinde, C.D., Kouabosso, A., Mbouma Bouassa, R.S., Longo, J.D., Kokanzo, E., Feissona, R., Gresenguet, G., Belec, L., 2016. J. Transl. Med. 14 (1), 326.
MSF Access Campaign, 2017, Putting HIV and HCV to the test. ⟨https://www.msfaccess.org/sites/default/files/HIV_Report_PuttingHIVHCVtotheTest_ENG_2017.pdf⟩ (accessed June 2018).
Pattanapanyasat, K., Sukapirom, K., Kowawisatsut, L., Thepthai, C., 2008. Cytom. B Clin. Cytom. 74, S98–S106.
Pham, M.D., Agius, P.A., Romero, L., McGlynn, P., Anderson, D., Crowe, S.M., Luchters, S., 2016. BMC Infect. Dis. 16 (1), 592.
Puchberger-Enengl, D., Krutzler, C., Keplinger, F., Vellekoop, M.J., 2014. Lab Chip 14 (2), 378–383.
Rodriguez, W.R., Christodoulides, N., Floriano, P.N., Graham, S., Mohanty, S., Dixon, M., Hsiang, M., Peter, T., Zavahir, S., Thior, I., Romanovicz, D., Bernard, B., Goodey, A.P., Walker, B.D., McDevitt, J.T., 2005. PLoS Med. 2 (7), e182.
Siepmann, J., Lecomte, F., Bodmeier, R., 1999. J. Control. Release 60 (2–3), 379–389.
Siepmann, J., Lecomte, F., Rathbone, J., 2012. Fundamentals and applications of controlled release. Drug Delivery, 1st ed. Springer, New York.
Singh, M., Haverinen, H.M., Dhagat, P., Jabbour, G.E., 2010. Adv. Mater. 22 (6), 673–685.
Stevens, D.Y., Petri, C.R., Osborn, J.L., Spicar-Mihalic, P., McKenzie, K.G., Yager, P., 2008. Lab Chip 8, 2038–2045.
Stringer, J., Derby, B., 2010. Langmuir 26 (12), 10365–10372.
Sysmex Partec, 2011, CyFlow® miniPOC. ⟨https://www.sysmex-partec.com/products/prdouct-detailview/cyflow-minipoc-3236.html⟩ (Accessed June 2018).
Tekin, E., Smith, P.J., Schubert, U.S., 2008. Soft Matter 4 (4), 703–713.
Tijero, M., Diez-Ahedo, R., Benito-Lopez, F., Basabe-Desmonts, L., Castro-Lopez, V., Valero, A., 2015. Biomicrofluidics 9, 044124.
UNAIDS, 2017, FACTSHEET – WORLDAIDSDAY 2017. ⟨http://www.unaids.org/sites/default/files/media_asset/UNAIDS_FactSheet_en.pdf⟩ (Accessed March 2018).
UNITAID - World Health Organization, 2012, HIV/AIDS Diagnostic Technology Landscape - 2nd edition. ⟨https://unitaid.eu/assets/UNITAID-HIV_Diagnostics_Landscape-2nd_edition.pdf⟩ (Accessed June 2018).
UNITAID - World Health Organization, 2015, HIV/AIDS Diagnostic Technology Landscape - 5th edition. ⟨http://www.unitaid.org/assets/UNITAID_HIV_Nov_2015_Dx_Landscape-1.pdf⟩ (Accessed June 2018).
Wade, D., Daneau, G., Aboud, S., Vercauteren, G.H., Urassa, W.S.K., Kestens, L., 2014. JAIDS-J. Acquir. Immune Defic. Syndr. 66 (5), e98–e107.
Wheeler, J.S.R., Longpré, A., Sells, D., McManus, D., Lancaster, S., Reynolds, S.W., Yeates, S.G., 2016. Polym. Degrad. Stab. 128 (Supplement C), 1–7.
World Health Organization, 2016, Consolidated guidelines on the use of antiretroviral drugs for treating and preventing HIV infection,) ⟨http://apps.who.int/iris/bitstream/handle/10665/208825/9789241549684_eng.pdf⟩ (Accessed June 2018).
Yakimets, I., Wellner, N., Smith, A.C., Wilson, R.H., Farhat, I., Mitchell, J., 2005. Polymer 46, 12577–12585.
Zhang, X., Wasserberg, D., Breukers, C., Terstappen, L.W., Beck, M., 2016a. ACS Appl. Mater. Interfaces 8, 27539–27545.
Zhang, X., Wasserberg, D., Breukers, C., Terstappen, L.W.M.M., Beck, M., 2016b. Analyst 141, 3068–3076.
Zhao, Z., Al-Ameen, M.A., Duan, K., Ghosh, G., Lo, J.F., 2015. Biosens. Bioelectron. 74, 305–312.
Zhu, H., Macal, M., Jones, C.N., George, M.D., Dandekar, S., Revzin, A., 2008. Anal. Chim. Acta 608 (2), 186–196.